

DEVELOPMENT AND ANALYSIS OF THE THEORY OF COMPOSITE EXPANSION RING UNDER ELECTROMAGNETIC LOADING

Zongxing Liu¹ & Jun Liu¹

¹ School of Aeronautics, Northwestern Polytechnical University

Abstract

The expansion ring test technology under electromagnetic loading is important to realize the high strain rate of tensile loading. The composite expansion ring loading scheme with low resistivity pusher to promote the specimen expansion loading makes the expansion ring test under electromagnetic loading realize the dynamic tensile loading of most materials. However, since this test method was proposed, the theory of composite expansion rings under electromagnetic loading has yet to develop fully. This paper analyzes the dynamic induction of the coil, pusher, and specimen during specimen expansion driven by the pusher. It comprehensively considers the influence of electric-magnetic-thermal-mechanical coupling during electromagnetic loading on the loading results. A compound theory that can predict the loading process of the composite expansion ring well is proposed, and a simplified compound theory is presented when the resistivity of the specimen is relatively large and the reliability of the theory is verified using numerical simulation methods. Based on the theory, the subsequent work will analyze several factors that affect electromagnetic loading efficiency, such as pusher material, loading circuit parameters, etc., and discuss the applicability of the simplified compound theory proposed in this paper. This study provides theoretical support for the design of the composite expansion ring under electromagnetic loading.

Keywords: Electromagnetic Load, Composite ring expansion, Compound theory, Simplified compound theory

1. Introduction

High-speed impact collision is a common mechanical problem in engineering and daily life. Researchers have realized that the response of objects under impact loads is significantly different from that under static loads, and the dynamic mechanical parameters of materials are crucial to predicting the mechanical response of materials under dynamic loads. Expansion ring technology is one of the important methods to measure the tensile mechanical properties of materials under high strain rate loading conditions [1], and the strain rate can reach the order of 10 4s⁻¹ [2]. The electromagnetic force is a body force; when the ring specimen is expanded by electromagnetic loading, the current on the specimen's cross-section is nearly uniform, which can effectively avoid the wave effect of mechanical loading [3]. The method can obtain reliable dynamic loading data for materials with low resistivity. However, many materials of interest to researchers have much higher resistivity than that of copper and aluminum, and the induced current is relatively small at the achievable loading voltage, making it difficult to achieve satisfactory loading results. Gourdin[3] proposed a composite loading scheme in which low resistivity materials were used to drive the expansion of general materials, which improved the application range of electromagnetic loading expansion ring technology, and 1100-F aluminum rings were used to drive tantalum samples for high strain rate loading tests.

The composite loading scheme of general materials driven by the low resistivity pusher can make the expansion ring test method of electromagnetic loading applicable to most materials for high strain rate tensile property testing. However, few studies have been on the loading theory since the birth of the composite expansion ring loading method. Since then, most researchers have followed this test idea to conduct high strain rate tensile loading tests, but few scholars have further developed the loading theory.

1

In this paper, the loading theory of the composite expansion ring is further developed. Considering the influence of induced current between the pusher and the specimen, and the dynamic induction between the coil, the pusher, and the specimen during the expansion process, the compound theory describing the loading process of the composite expansion ring is proposed. Reasonable simplification is carried out when the resistivity of the specimen material is relatively large, the simplified compound theory of expansion ring is obtained. Using numerical simulation, the theory proposed in this paper is verified. In the follow-up study, we will discuss the material selection of the pusher and the influence of electromagnetic loading parameters on the loading efficiency, and the applicability of simplified compound theory will be discussed based on compound theory and simplified compound theory.

2. Composite Expansion Ring Loading Theory

In 1963, Johnson et al. [4] proposed the explosive expansion ring test technology in a pioneering way, which used the explosion impact load to drive the specimen expansion, the principle of which is shown in Fig. 1. After the effect of explosion load, the sample is in a state of uniaxial stress. The stress, strain, and strain rate of the specimen at this stage can be described according to equations (1), (2), and (3), respectively.

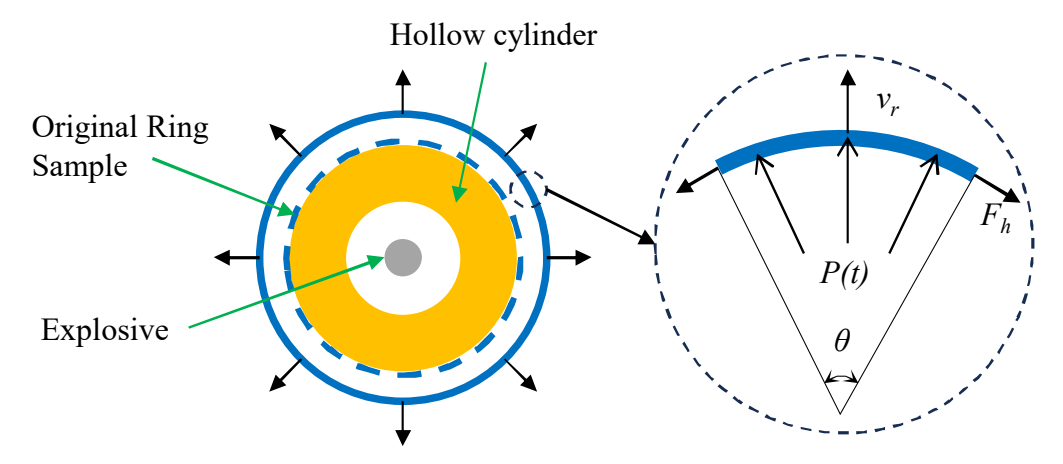


Fig. 1: Schematic diagram of expansion ring principle

$$\sigma = \rho r a_r$$
 (1)

$$\varepsilon = \ln(r/r_0) \tag{2}$$

$$\dot{\varepsilon} = \frac{d\varepsilon}{dt} = \frac{1}{r}\frac{dr}{dt} = \frac{v_r}{r} \tag{3}$$

In the above formula, ρ is the density of the sample, r is the radius of the sample, a_r is the radial acceleration of the sample, r_0 is the initial radius of the sample, and v_r is the radial velocity.

Niordson[5] first proposed a high strain rate loading method to achieve ring expansion by electromagnetic loading. Gourdin [3] significantly contributed to this technology's practical development. Fig. 2 shows the schematic diagram of the loading principle of a general specimen driven by the low resistance pusher under electromagnetic force loading.

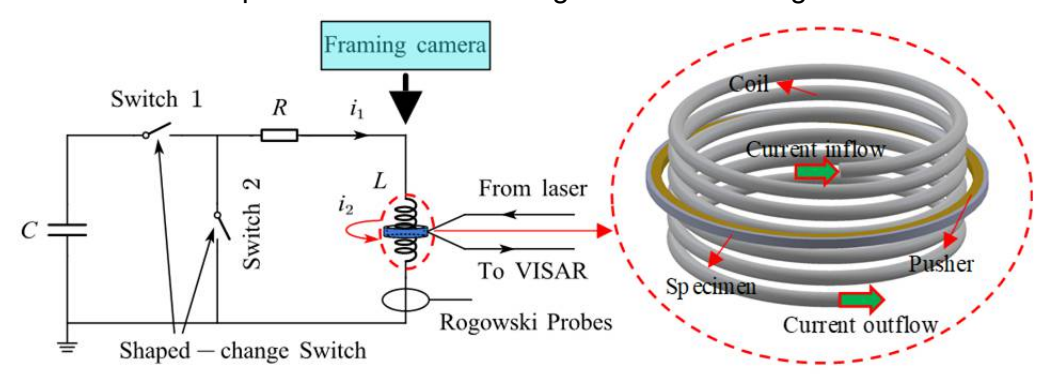


Fig. 2: Schematic diagram of electromagnetic drive principle

2.1 Compound theory

The electromagnetic drive loading circuit can be regarded as three equivalent circuits, RLC discharge circuit, pusher induction circuit, and specimen induction circuit. The voltage relationship between the RLC discharge circuit and the induction circuit can be described as follows:

$$\begin{cases} V + R_{c}I_{c} + L_{c}\frac{dI_{c}}{dt} + \frac{d(M_{cs}I_{s})}{dt} + \frac{d(M_{cp}I_{p})}{dt} = 0 \\ R_{p}I_{p} + \frac{d(L_{p}I_{p})}{dt} + \frac{d(M_{cp}I_{c})}{dt} + \frac{d(M_{sp}I_{s})}{dt} = 0 \end{cases}$$

$$\begin{cases} R_{s}I_{s} + \frac{d(L_{s}I_{s})}{dt} + \frac{d(M_{cs}I_{c})}{dt} + \frac{d(M_{sp}I_{p})}{dt} = 0 \end{cases}$$

$$(4)$$

$$\frac{dV}{dt} = \frac{I_c}{C} \tag{5}$$

Where V is the capacitor voltage, C is the capacitor capacitance, R_c is the equivalent resistance of the discharge loop, R_s is the equivalent resistance of the specimen, R_p is the equivalent resistance of the pusher, I_c is the current of the discharge loop, I_s is current on the specimen, I_p is current on the pusher, L_c is the self-inductance of the specimen, L_p is the self-inductance of the pusher, M_{cs} is the mutual inductance between the coil and the specimen, M_{cp} is the mutual inductance between the specimen and the pusher. By finishing and transforming formula (4), we can obtain:

$$\frac{dI_{c}}{dt} = \frac{\kappa_{1}(M_{sp} - L_{s}L_{p}) + \kappa_{2}(L_{p}M_{cs} - M_{cp}M_{sp}) + \kappa_{3}(L_{s}M_{cp} - M_{cs}M_{sp})}{L_{s}M_{cp}^{s} + L_{p}M_{cs}^{2} + L_{c}M_{sp}^{s} - 2M_{cs}M_{cp}M_{sp} - L_{c}L_{s}L_{p}}$$

$$\frac{dI_{s}}{dt} = \frac{\kappa_{1}(L_{p}M_{cs} - M_{cp}M_{sp}) + \kappa_{2}(M_{cp}^{s} - L_{c}L_{p}) + \kappa_{3}(L_{c}M_{sp} - M_{cs}M_{cp})}{L_{s}M_{cp}^{s} + L_{p}M_{cs}^{2} + L_{c}M_{sp}^{s} - 2M_{cs}M_{cp}M_{sp} - L_{c}L_{s}L_{p}}$$

$$\frac{dI_{p}}{dt} = \frac{\kappa_{1}(L_{s}M_{cp} - M_{cs}M_{sp}) + \kappa_{2}(L_{c}M_{sp} - M_{cs}M_{cp}) + \kappa_{3}(M_{cs}^{s} - L_{c}L_{s})}{L_{s}M_{cp}^{s} + L_{p}M_{cs}^{2} + L_{c}M_{sp}^{s} - 2M_{cs}M_{cp}M_{sp} - L_{c}L_{s}L_{p}}$$
(6)

In the formula κ_1 , κ_2 and κ_3 are shown below :

$$\begin{cases} \kappa_{1} = -V - R_{c}I_{c} - \frac{dM_{cs}}{dr}v_{r}I_{s} - \frac{dM_{cp}}{dr}v_{r}I_{p} \\ \kappa_{2} = -R_{s}I_{s} - \frac{dL_{s}}{dr}v_{r}I_{s} - \frac{dM_{cs}}{dr}v_{r}I_{c} - \frac{dM_{sp}}{dr}v_{r}I_{p} \end{cases}$$

$$(7)$$

$$\kappa_{3} = -R_{p}I_{p} - \frac{dL_{p}}{dr}v_{r}I_{p} - \frac{dM_{cp}}{dr}v_{r}I_{c} - \frac{dM_{sp}}{dr}v_{r}I_{s}$$

In the electromagnetic loading stage, the pusher drives the specimen to accelerate, and the radial acceleration and radial velocity of the specimen and the pusher are the same. The total energy of the discharge loop, the pusher loop, and the specimen loop can be described by the following equation:

$$W = \frac{1}{2}CV^{2} + \int_{0}^{t} \left(R_{c}I_{c}^{2} + R_{s}I_{s}^{2} + R_{p}I_{p}^{2} \right) dt + \frac{1}{2} \sum_{i=1}^{3} \sum_{j=1}^{3} L_{ij}I_{i}I_{j} + \frac{1}{2}m_{sp}v_{r}^{2} + \sum_{k=1}^{2} \int_{0}^{t} 2\pi A_{k}v_{r}\sigma_{k}(\varepsilon) dt$$
(8)

In the formula, m_{sp} is the total mass of the driving ring and the sample. During the loading process, the energy of the whole system is conserved, and there is no energy exchange with the outside world, that is dW=0. The acceleration of the sample ring during the loading process can be described as follows:

$$\frac{dv_{r}}{dt} = \frac{1}{m_{sp}} \left[\frac{I_{s}^{2}}{2} \frac{dL_{s}}{dr} + \frac{I_{p}^{2}}{2} \frac{dL_{p}}{dr} + I_{c}I_{s} \frac{dM_{cs}}{dr} + I_{c}I_{p} \frac{dM_{cp}}{dr} + I_{s}I_{p} \frac{dM_{sp}}{dr} - 2\pi \left(A_{s}\sigma_{s} + A_{p}\sigma_{p} \right) \right]$$
(9)

The following formula can describe the temperature T of the pusher and the specimen.

$$\frac{dT}{dt} = \frac{I^2 R}{c_p m} + \frac{\sigma \dot{\varepsilon}_p}{c_p \rho} \tag{10}$$

2.2 Simplified compound theory

According to Faraday's electromagnetic induction principle, the induced electromotive force generated by the specimen and the pusher under the action of the changing magnetic field of the coil should meet $V_s \approx V_p$, and V_p is slightly greater than V_s . If the resistivity of the specimen material is assumed to be ten times that of the pusher material, even if the specimen has a smaller cross-section, and a longer length, the induced current on the specimen is only 1/10 of the induced current on the

pusher. At this point, the induced current on the specimen can be ignored. It is approximately considered that the specimen with a high resistivity is an insulating material, $I_s=L_s=M_{cs}=M_{sp}=0$ in equation (4). Under this assumption, the current in the RLC discharge loop and the induction loop of the drive ring can be described as follows:

$$\begin{bmatrix}
\frac{dI_c}{dt} = \frac{1}{M_{cp}^2 - L_c L_p} \left[L_p \left(R_c I_c + I_p v_r \frac{dM_{cp}}{dr} + V \right) - M_{cp} \left(R_p I_p + I_c v_r \frac{dM_{cp}}{dr} + I_p v_r \frac{dL_p}{dr} \right) \right] \\
\frac{dI_p}{dt} = \frac{1}{M_{cp}^2 - L_c L_p} \left[L_c \left(R_p I_p + I_p v_r \frac{dL_p}{dr} + I_c v_r \frac{dM_{cp}}{dr} \right) - M_{cp} \left(V + R_c I_c + I_p v_r \frac{dM_{cp}}{dr} \right) \right]$$
(11)

During the loading phase of the electromagnetic drive, the radial velocity of the specimen and the pusher can be described as follows:

$$\frac{dv_r}{dt} = \frac{1}{m_{sp}} \left[\frac{I_p^2}{2} \frac{dL_p}{dr} + I_c I_p \frac{dM_{cp}}{dr} - 2\pi \left(A_s \sigma_s + A_p \sigma_p \right) \right]$$
(12)

3. Theoretical verification

The parameters of the RLC circuit loaded by the electromagnetic drive are shown in Table 1. The helical coil is wound with copper wire. Considering the wire resistance and parasitic inductance connected to the helical coil, the theoretical model is verified based on the loading circuit.

Table 1: RLC circuit parameters								
	k	n	r_L	r_{AL}	R_w	L_p	С	V
Value	2.3 mm	6	14.1 mm	2 mm	39.6 mΩ	0.3198 µH	56.4 µF	4 kV

In the table, k represents the pitch of coil turns, n represents the number of coil turns, r_L is the radius of coil wire, r_{AL} is the cross-section diameter of coil wire, R_W is the resistance of conductor resistance, L_P is the parasitic inductance of circuit wire, C is the capacitor capacitance, and V is the initial voltage of the capacitor. Specimen and pusher dimensions are shown in Fig. 3.

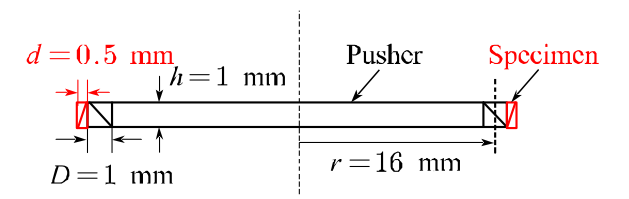


Fig. 3: Specimen and pusher dimensions

In theoretical verification, the material of the specimen and the pusher is selected as copper, and the specimen is assumed to be an insulating material when verifying the simplified compound theory, that is, the $R_{\Omega s}$ of the specimen is considered to be ∞ . Table 2 shows the parameter values of the physical properties of copper, ρ is the density of the material, R_{Ω} is the material's resistivity, cp represents the material's specific heat capacity, T is the sample temperature, and unit is K.

Table 2: Physical properties of copper ¹⁷							
$ ho$ kg/m ³ R_{Ω} Ω ·m cp J /(kg·K)							
Copper	8924	1.7×10 ⁻⁸ [1+0.0039(T-273)]	0.092×T+356.4				

The mechanical properties of the tested material were determined by the Johnson-Cook model which considered the strain rate hardening effect and temperature softening effect. The parameters of the Johnson-Cook model for copper are shown in Table 3.

Table 3: Johnson-Cook model parameters for copper [/]								
Materials	A	MPa	В	MPa	n	С	m	<i>T_m</i> °C
Copper		69	2	223.56	0.31	0.025	1.09	1356

The commercial software LS-DYNA was used to simulate the electromagnetic loading process, and the loading spiral, sample, and driving ring models were established, as shown in Fig. 4.

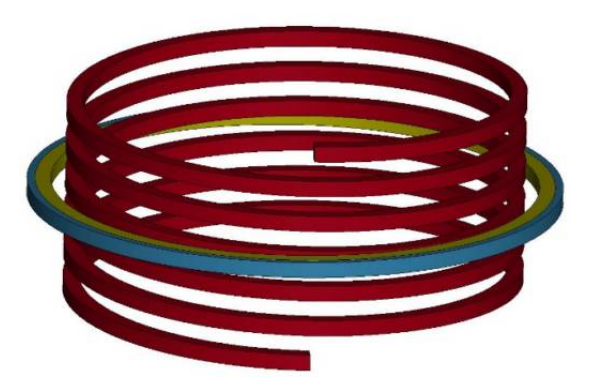


Fig. 4: Numerical simulation model

Define relative errors as follows:

$$E_r = \frac{|f_s - f_t|}{f_t} \tag{13}$$

In the formula, f_s represents the numerical simulation results of this article, and f_t represents the theoretical prediction results.

The predicted results of the loading process by expansion ring compound theory and numerical simulation method are shown in Fig. 5. The trend and peak value of current, velocity, and temperature obtained by the compound theory and numerical simulation are in good agreement.

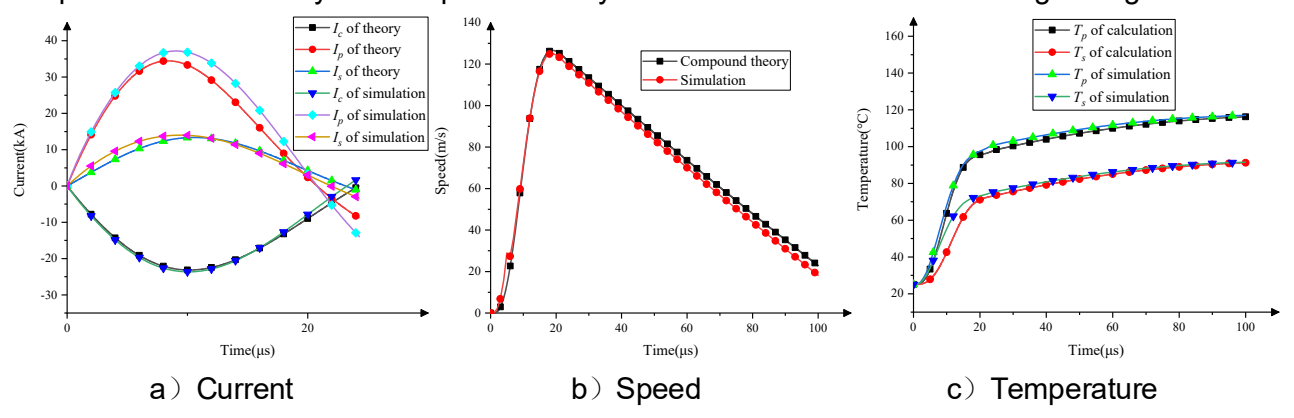


Fig. 5: Comparison of prediction results of compound theory

The peaks and relative errors of current, speed, and temperature obtained through theoretical and numerical simulation are shown in Table 4.

Table 4: Comparison of peak prediction results of the expansion ring compound theory

	I _c	I _p	Is	v_r	T_{ρ}	Ts
Simulation	23.6 kA	37.2 kA	14 kA	125.1 m/s	117 ℃	91.6 °C
Theory	23.1 kA	34.5 kA	13.3 kA	126.6 m/s	116.2 ℃	91.2 ℃
E _r	2.1	7.2	5	1.2	0.7	0.4

Ignoring the specimen current, the simplified compound theory and numerical simulation method of the expansion ring were used to predict the loading process, as shown in Fig. 6.

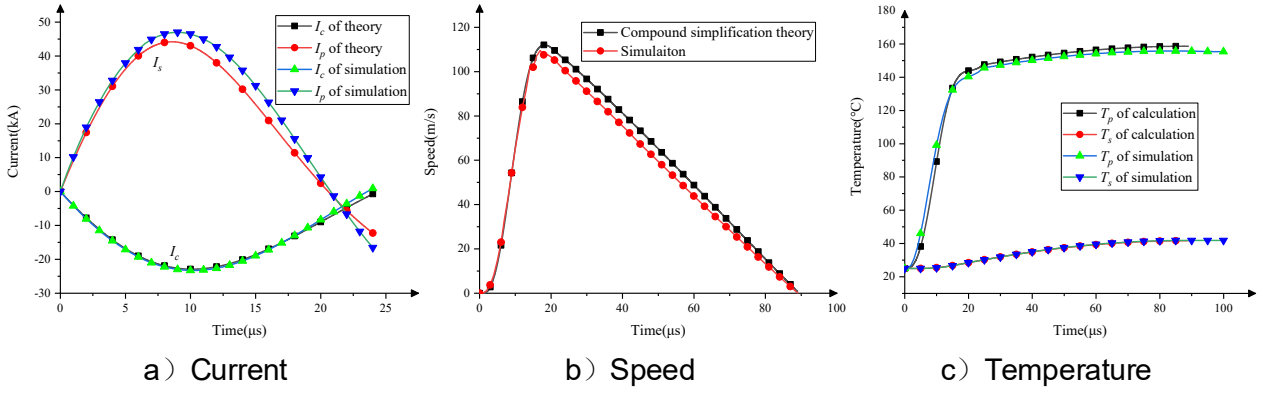


Fig. 6: Comparison of prediction results of simplified compound theory

The peaks and relative errors of current, speed, and temperature obtained through theoretical and numerical simulation are shown in Table 5.

Table 5: Comparison of peak prediction results of the expansion ring simplified compound theory

	Ic	Ιp	v_r	$T_{ ho}$	Ts
Simulation	23.3 kA	47 kA	112 m/s	155.3 ℃	41.8 °C
Theory	22.9 kA	44.2 kA	109.5 m/s	158.7 ℃	41.7 ℃
Relative error	1.7	5.9	2.2	2.2	1.2

The numerical simulation method is used to verify the theory proposed in this paper. The maximum relative error of the compound theory is 7.2%, and the maximum relative error of the simplified compound theory is 5.9%, which shows the rationality of the theory proposed in this paper.

4. Patterns of influence from factors in composite pusher-specimen experiments

The composite pusher-specimen loading scheme, which uses a low-resistivity pusher to drive a high-resistivity specimen, significantly expands the application scope of electromagnetic loading expansion ring test technology. Many factors can influence the loading results when using this scheme. Based on the RLC circuit shown in Table 1 and the dimensions of the pusher and specimen shown in Fig. 3, this study explores the patterns of how various factors affect the composite pusher-specimen experiment.

4.1 Pusher material

Equation (9) indicates that the induced current, density, and stress-strain relationship of the pusher all affect the change in expansion velocity. When using the composite pusher-specimen loading scheme, at the same loading voltage, materials with high resistivity can achieve greater expansion velocity, thus enhancing loading efficiency. The material of the pusher significantly influences the loading results. Table 7 displays the resistivity and density of some materials at 25 °C.

Table 7 Resistivity and density of materials

Material	Silver	Copper	Gold	Aluminum	Magnesium
Resistivity (10 ⁻⁸ Ω·m)	1.5	1.7	2.065	2.655	4.47
ρ (kg/m³)	10500	8924	19300	2700	1740

Silver and gold, as pure metals with very low resistivity at room temperature, would undoubtedly be excellent if only considering the influence of induced current on the electromagnetic loading process. However, both silver and gold are typical heavy metals; silver's density is nearly four times that of aluminum, and gold's density exceeds aluminum's by more than seven times. Compared to general metals, silver is relatively soft, making it unsuitable for use as a pusher to expand other materials. Additionally, gold has a higher resistivity than copper, a higher density, and being a typical precious metal, it is costly, these factors determine that gold is also unsuitable as a pusher material. Copper is the best conductor of electricity after silver, yet it is also a typical heavy metal with a relatively high density; Magnesium has the lowest density among low-resistivity metals (excluding metallic sodium, which is not considered due to its melting point of only 97°C), however, it has the highest resistivity among low-resistivity metals; Compared to copper and magnesium, aluminum's density is only about 0.3 times that of copper, and its resistivity is approximately 0.6 times that of magnesium. Copper, aluminum, and magnesium each have unique advantages as materials for pushers. Their physical properties and Johnson-Cook model parameters are displayed in Tables 8 and 9, respectively.

Table 8 Physical properties of common materials [8]

Materials	ρ (kg/m ³)	$R_{\Omega}(\Omega \cdot m)$	<i>cp</i> (J /(kg⋅K))
Magnesium	1740	4.47×10 ⁻⁸ [1+0.0041(T-273)]	0.6047×T+800.6
Aluminum	2700	2.655×10 ⁻⁸ [1+0.00423(T-273)]	0.61×T+671.5
Cast iron	7870	9.7×10 ⁻⁸ [1+0.006(T-273)]	0.4743×T+297.2

Table 9 Johnson-Cook model parameters of common materials

Materials	A(MPa)	B(MPa)	n	С	m	<i>T_m</i> (°C)
Magnesium [9]	118	15.399	0.919	0.08091	1.517	650

Aluminum [10]	140	75.2	0.6474	0.0125	1	660
Cast iron [11]	270	275	0.35	0.0042	1.23	1535

Copper, aluminum, and magnesium were used as materials for the pusher, with cast iron, a typical high-resistivity material, used as the specimen. The physical properties and Johnson-Cook model parameters of cast iron are displayed in Tables 8 and 9, respectively. Based on the electromagnetic loading theory of the composite pusher-specimen, the predicted results of the loading process are shown in Fig. 7; the peak velocities achieved by driving cast iron with copper, aluminum, and magnesium are 113.9 m/s, 164.2 m/s, and 132.2 m/s, respectively. Under the same conditions, aluminum as the pusher achieved the highest expansion velocity, indicating that aluminum provides higher loading efficiency than copper and magnesium. When using the composite pusher-specimen loading scheme, low-resistivity, high-strength aluminum alloys have more practical value compared to copper and magnesium alloys. Subsequent analysis will focus on the choice of aluminum for the pusher and cast iron for the specimen, exploring how various factors influence the composite pusher-specimen loading process.

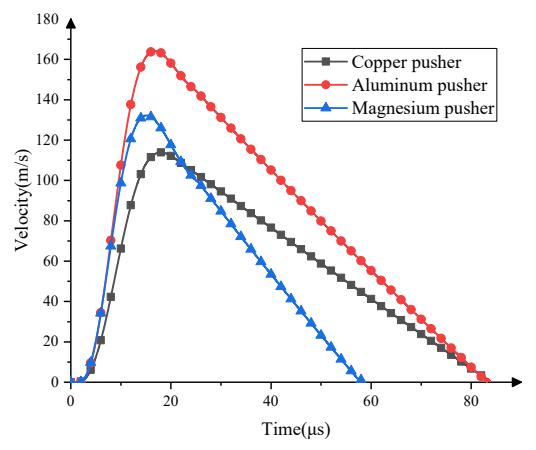


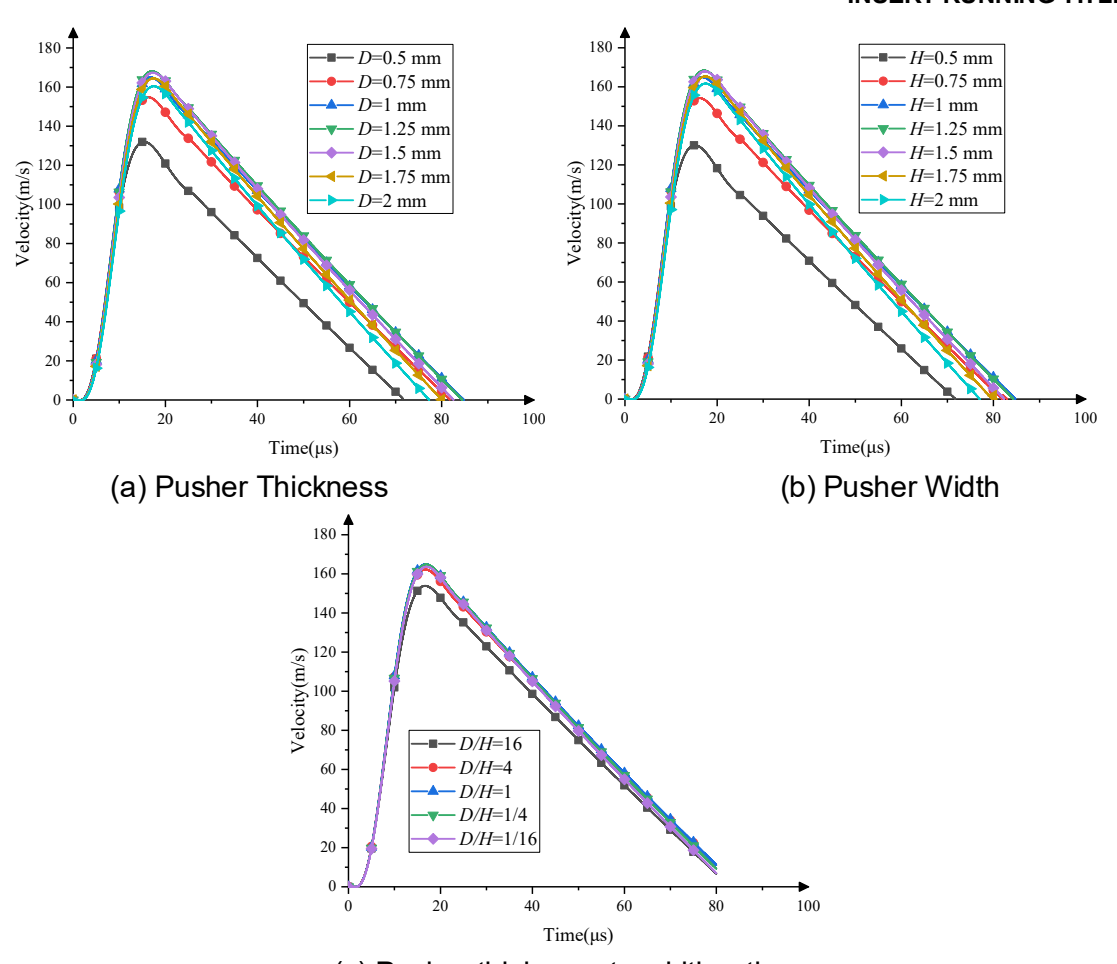
Fig. 7 The influence of pusher material on the loading process

4.2 Pusher geometric parameters

The geometric parameters of the pusher consider three influencing factors: the thickness D, the width H, and the thickness-to-width ratio D/H. When analyzing the thickness-to-width ratio, the cross-sectional area of the pusher is maintained at 1 mm². Initial gaps between the pusher and the specimen are not considered, meaning that the loading process conforms to the relationship described in Equation (14).

$$r_p = r - \frac{1}{2}(d+D)$$
 (14)

The theoretical analysis results of the composite pusher-specimen loading with different geometric parameters of the pusher are shown in Fig. 8. As can be seen from Fig. 8(a) and Fig. 8(b), a smaller thickness *D* and width *H* of the pusher led to a decrease in peak velocity. This is because the reduction in the thickness and width of the pusher results in a smaller cross-sectional size, increased pusher resistance, and reduced induced current. It is also noteworthy that a smaller cross-sectional area of the pusher corresponds to a smaller mass of the pusher. Although the resistance decreases and the induced current increases when the cross-sectional size of the pusher is larger, the peak velocity of the specimen no longer increases significantly once the thickness and width of the pusher exceed 1 mm. Within the studied range of pusher sizes, larger thicknesses and widths of the pusher have a negligible impact on the loading results. Furthermore, a larger thickness-to-width ratio also weakens the loading capacity of the composite pusher-specimen, as shown in Fig. 8(c).



(c) Pusher thickness-to-width ratio Fig. 22 Pusher geometric parameters influence

5. Summary and Outlook

As an extended abstract, this paper gives an overview of the author's work. In this paper, the expansion ring compound theory for predicting electromagnetic loading and the simplified compound theory when the specimen resistance is large are proposed, and the rationality of the proposed theory is verified by the numerical simulation method.

Based on the theory proposed in this paper, using cast iron materials as specimens, the effects of pusher materials and pusher sizes on the results of electromagnetic loading are examined, providing guidance for the design of electromagnetic loading tests with composite pusher-specimen.

Copyright Statement

The authors confirm that they, and/or their company or organization, hold copyright on all of the original material included in this paper. The authors also confirm that they have obtained permission, from the copyright holder of any third party material included in this paper, to publish it as part of their paper. The authors confirm that they give permission, or have obtained permission from the copyright holder of this paper, for the publication and distribution of this paper as part of the ICAS proceedings or as individual off-prints from the proceedings.

References

- [1] Sia Nemat-Nasser. Introduction to high strain rate testing. ASM Handbook. 8. 2000, 427-428.
- [2] J E Reaugh. Computer simulation and analysis of the expanding ring test. Shock Waves in Condensed Matter, 1986: 395-399.
- [3] W H Gourdin, S L Weinland, RM Boling. Development of the electromagnetically launched expanding ring as a high-strain-rate test technique. Review of Scientific Instruments, 1989, 60(3): 427-432.
- [4] P C Johnson, B A Stein, R S Davis. Measurement of dynamic plastic flow properties under uniform stress. Symposium on the dynamic behavior of materials. ASTM Special Publication, No. 336, 1963: 195-198.

INSERT RUNNING TITLE HERE

- [5] Niordson FI. A unit for testing materials at high strain rates. Experimental Mechanics. 1965, 5(1): 29-32.
- [6] W H Gourdin. Analysis and assessment of electromagnetic ring expansion as a high-strain-rate test. Journal of Applied Physics, 1989, 65(2): 411-422.
- [7] D. L. Littlefield. The Effect of Electromagnetic Fields on Taylor Anvil Impacts. 20th International Symposium of Ballistics, Orlando, Florida, 2002.
- [8] LB Li, YF Sun. Handbook of Physical Properties of Metal Materials, China Machine Press, 2011.
- [9] Rohit Jain, Harsh Soni, RP Mahto et al. An insight into high-temperature deformation mechanism of magnesium in-situ composite through development of Johnson-Cook and constitutive model. International Journal of Lightweight Materials and Manufacture, 2023, Vol. 6(4): 574-588.
- [10]Peter Grpche, Christian Pabst. Numerical Simulation of Impact Welding Processes with LS-DYNA.10th European LS-DYNA Conference, Würzburg, 2015.
- [11]S Rolc, J Buchar. Effect of the Temperature on the Ballistic Efficiency of Plates.22nd International Symposium of Ballistics, Vancouver, Canada, 2005.

9